Journal of MATERIALS RESEARCH

Article
DOI:10.1557/s43578-020-00045-w

ADVANCED NANOMECHANICAL TESTING

FOCUS ISSUE

Applicability of focused Ion beam (FIB) milling with gallium, neon, and xenon to the fracture toughness characterization of gold thin films

Eva I. Preiß[1], Benoit Merle[1,a)], Yuan Xiao[2], Florentina Gannott[3], Jan P. Liebig[1], Jeffrey M. Wheeler[2], Mathias Göken[1]

[1] *Materials Science & Engineering, Institute I and Interdisciplinary Center for Nanostructured Films (IZNF) Erlangen, Friedrich-Alexander-Universität Erlangen-Nürnberg (FAU), Erlangen, Germany*
[2] *Laboratory for Nanometallurgy, ETH Zürich, Zurich, Switzerland*
[3] *Technology Development and Service Unit for Nanostructuring, Max-Planck-Institute for the Science of Light, Erlangen, Germany*
[a)] Address all correspondence to this author. e-mail: benoit.merle@fau.de

Received: 3 October 2020; accepted: 4 December 2020; published online: 16 February 2021

Benoit Merle and Mathias Göken were editors of this journal during the review and decision stage. For the JMR policy on review and publication of manuscripts authored by editors, please refer to http://www.mrs.org/editor-manuscripts/

Focused ion beam (FIB) milling is an increasingly popular technique for fabricating micro-sized samples for nanomechanical characterization. Previous investigations have cautioned that exposure to a gallium ion beam can significantly alter the mechanical behavior of materials. In the present study, the effects of gallium, neon, and xenon ions are scrutinized. We demonstrate that fracture toughness measurements on freestanding gold thin films are unaffected by the choice of the ion species and milling parameters. This is likely because the crack initiation is controlled by the local microstructure and grain boundaries at the notch, rather than by the damaged area introduced by FIB milling. Additionally, gold is not susceptible to chemical embrittlement by common FIB ion species. This confirms the validity of microscale fracture measurements based on similar experimental designs.

Introduction

Focused ion beam milling (FIB) has fundamentally changed nanomechanical testing, inasmuch as it has allowed unprecedented experimental designs, which are useful for targeting specific material properties at the nanometer scale [1, 2]. For example, FIB-machined samples were pivotal to the discovery of geometric size effects on strength [3–20]. FIB-based techniques also have the unique ability to isolate and investigate the mechanical contribution of microstructural features and defects—such as grain and twin boundaries [21–25]—and are increasingly used to study the fracture mechanisms at the nanometer scale, for instance in thin films [26–31]. The increasing popularity of FIB techniques has continued, despite concerns voiced from the very beginning over possible detrimental side effects of the ion milling process. Kiener et al. evidenced significant damage to the crystal structure of processed samples, ranging from the nucleation of defects and dislocations to the implantation of ions [32]. This damage has the potential to significantly affect the mechanical properties of the samples. In the worst case, Shim et al. evidenced a drop in strength in a single crystal by one order of magnitude [33, 34]. Polycrystals are also affected when the ion species segregates at the grain boundaries and forms a ductile phase. In such a case, Xiao et al. evidenced a drop in strength in aluminum micropillars because of the formation of a eutectic Ga-Al phase at the grain boundaries [35, 36]. Some strategies for mitigating FIB damage have already been suggested, such as shadow milling [12, 37] or post-treatment annealing [38, 39], but they are neither universally effective nor widely used yet. For the time being, most studies merely rely on the assumption that the pristine structure of the samples is preserved throughout the milling process. The

© The Author(s) 2021

aim of the present study is to investigate whether valid measurements of the fracture properties of thin films are possible—for instance by bulge testing [40–42]—and to determine the influence, if any, of the ion species and milling process used.

Results

Effect of ion species

The investigations focused on 100–300 nm gold membranes obtained by thermal evaporation. In order to study the influence of ion species on the measured fracture toughness of these films, specimens obtained from a single deposition batch were selectively notched with gallium, neon, or xenon FIBs. Details on the experimental procedure are provided in the "Materials and Methods" section. Representative micrographs showing the notch geometry obtained with each ion species are provided in Fig. 1a–c. Ne-FIB and Xe-FIB yielded the sharpest and the bluntest notches, respectively.

The fracture toughness of the corresponding membranes was measured using bulge tests [40–42] and plotted in Fig. 2. Irrespective of the ion species, the fracture toughness data exhibit a correlation with the film thickness. The slightly increasing trend in the Ne-FIB data corresponds to the expectations from Bluhm's and Knott's models [43, 44], as well as from previous observations based on Ga-FIB sample preparation [26, 45]. For all conditions, the scattering of the data in Fig. 2 is rather low and consistent with the few FIB-free fracture experiments on thin films reported in the literature [46–48]. In line with expectations, thinner films exhibit a greater scattering than their thicker counterparts, presumably due to a greater contribution from their surface roughness [28], which introduces some randomness. Because the curves for different ion species partially overlap, it is virtually impossible to ascertain any effect of the fabrication process on the fracture toughness measurements. Note that the Xe-FIB samples—which only encompass three 250 nm samples—fall very well in line with the Ga-FIB ones. While the Ga-FIB and Xe-FIB measurements are virtually indistinguishable, Ne-FIB exhibits some discrepancies. However, there is no consistent trend throughout the investigated thickness range. Possible explanatory approaches and implications for this apparent contradiction are discussed in the next section.

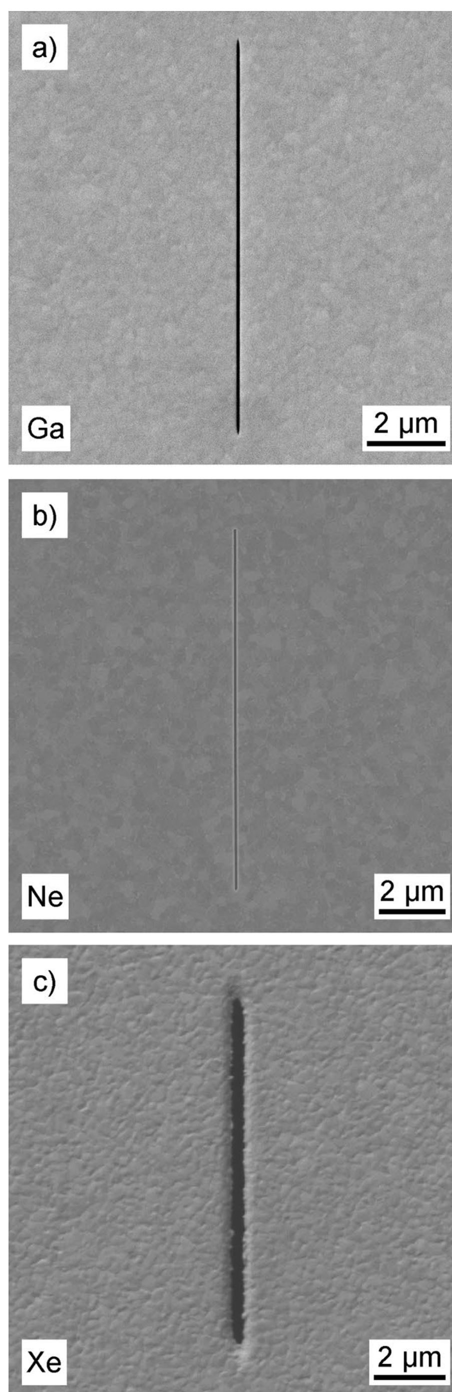

Figure 1: Secondary electron micrographs of notched gold films prepared with different FIB ion species: (a) conventional Ga-FIB with 30 kV and 10 pA (b) Ne-FIB with 25 kV and 5 pA (c) Xe-FIB with 30 kV and 100 pA.

Effect of notch radius

Figure 1a–c illustrates how strongly the geometry of the slit is influenced by the FIB ion species, with the Xe-FIB notches being considerably blunter than the other two ion species. The different notch radii should in theory influence the measurements, as a blunt tip should lead to an overestimation of the fracture toughness [47, 49, 50]. The effect of the notch radius was investigated in practice by structuring a 150-nm gold sample with an intentionally blunt notch of ca. 500 nm radius. Its fracture behavior was compared to reference samples with sharper notches of ca. 100 nm radius, which had been produced using the same Ga-FIB technique, see Fig. 3a, b. Against expectations, the fracture toughness did not increase with a

© The Author(s) 2021

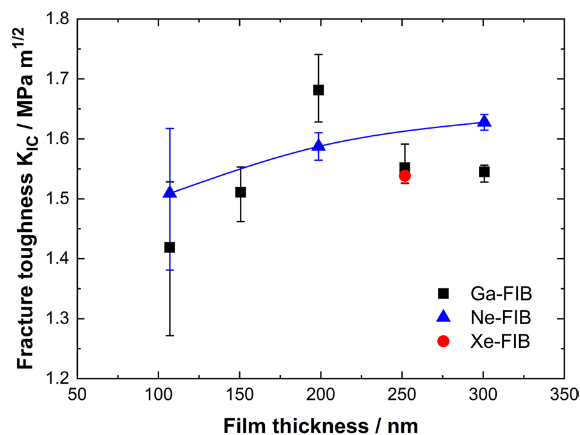

Figure 2: Measured fracture toughness as a function of the specimen thickness and the ion species used for structuring the samples. The error bars correspond to the minimum and maximum values measured for each condition (2–4 individual tests).

blunter notch, but rather—slightly—decreased from ca. 2.0 to 1.9 MPa $m^{1/2}$ (see Fig. 3d). This observation suggests that the notch tip radius does not play any significant role in polycrystalline gold films. In the next section, we will investigate whether the FIB-milling process itself matters.

Effect of ion damage

Scanning transmission electron (STEM) micrographs indeed evidence a FIB-damaged region around the notch. The clustering of crystallographic defects typically results in dark spots on the STEM image, such as those visible ahead of the notch in Fig. 4, which corresponds to dislocation loops and implanted point defects. With the investigated 56-nm-thick gold specimen, a significant concentration of defects can be observed as far as 400 nm away from the notch tip. They rapidly fade away at larger distances. This lateral spread of the damage zone is unexpectedly high when compared to SRIM (stopping range of ions in matter) [51] or molecular dynamics [52] simulations, which are usually regarded as reliable predictions [32, 53]. With the experimental parameters of this study, the SRIM simulations shown in Fig. 5 predict a damage radius of 5–25 nm only. In practice, gallium implantation should also be limited to a very thin amorphous layer at the surface [32, 54, 55], provided the ion beam is perfectly focused and the FIB apertures are in pristine condition. However, gallium is likely to be implanted in a wider zone if extensive beam tails are present, as it is the case here. The combination of a high point defect density and local heating by the ion beam might additionally increase the diffusion rate and lead to a wider lateral spread of the implanted gallium ions [56]. In any case, the 400-nm damage zone remains small compared to the 10 μm length of the slit.

It is usually assumed that FIB damage mechanically weakens [33, 34, 42, 57] the area around the notch and thus reduces the fracture toughness of the membrane. This hypothesis is consistent with our previous AFM observation [26] of brittle fracture processes taking place locally at the notch tip, while a more ductile deformation dominates away from it. In the present study, we attempted to selectively avoid FIB effects by creep loading some FIB-notched samples prior to fracture testing. Creep deformation yielded an intergranular crack extending past the FIB-affected area (see Fig. 3c). Although subsequent bulge testing led to significantly higher K_{IC} values than for plain FIB notches (see Fig. 3d), it is questionable whether the difference can be ascribed to FIB effects. Indeed, the creep-induced cracks are prone to crack branching and crack deflection along grain boundaries oriented perpendicularly to the crack (see Fig. 3c), which could also account for the apparent toughening.

In any case, note that the STEM micrograph shown in Fig. 4 originates from an extremely thin specimen—in order to ensure electron transparency at 30 keV—and therefore corresponds to a lower bound of damage density. Structuring thicker films require higher gallium doses in order to mill notches through the whole gold layer, which has been shown by Kiener et al. to increase the concentration of gallium in the vicinity of the FIB-milled area [32]. In the case of gold, a critical concentration of solute gallium above which it segregates to grain boundaries, as seen in aluminum [58], cannot be ruled out. Due to the low solubility of gallium in gold at room temperature (ca. 3 at. %), brittle intermetallic AuGa phases might form as well [59]. Both the brittle AuGa phases and the embrittled grain boundaries have the potential to limit the fracture toughness of the films, which might explain why its increase slows down at large film thicknesses (see Figs. 2 and 3).

Discussion

It is well known that FIB-induced damage can influence the mechanical behavior of small-scale samples. This can result from a number of different types of FIB damage: knock-on damage-induced dislocations [32], implanted ions [32, 60], and gallium embrittlement [35]. Dislocation loops and point defects implanted by FIB can increase the strength of materials through Taylor hardening. Strengthening is usually regarded as detrimental to the ductility of face-centered cubic metals, but this does not hold true for polycrystalline thin films. Indeed, we previously showed that the fracture toughness scales with the yield strength, because the latter controls the necking behavior that is critical for crack propagation [28]. FIB damage from ion implantation would result in a further toughening effect, as the compressive residual stress induced by the strain from the implanted ions would act to resist crack nucleation [60]. These implanted residual stresses scale with the Young's modulus of

© The Author(s) 2021

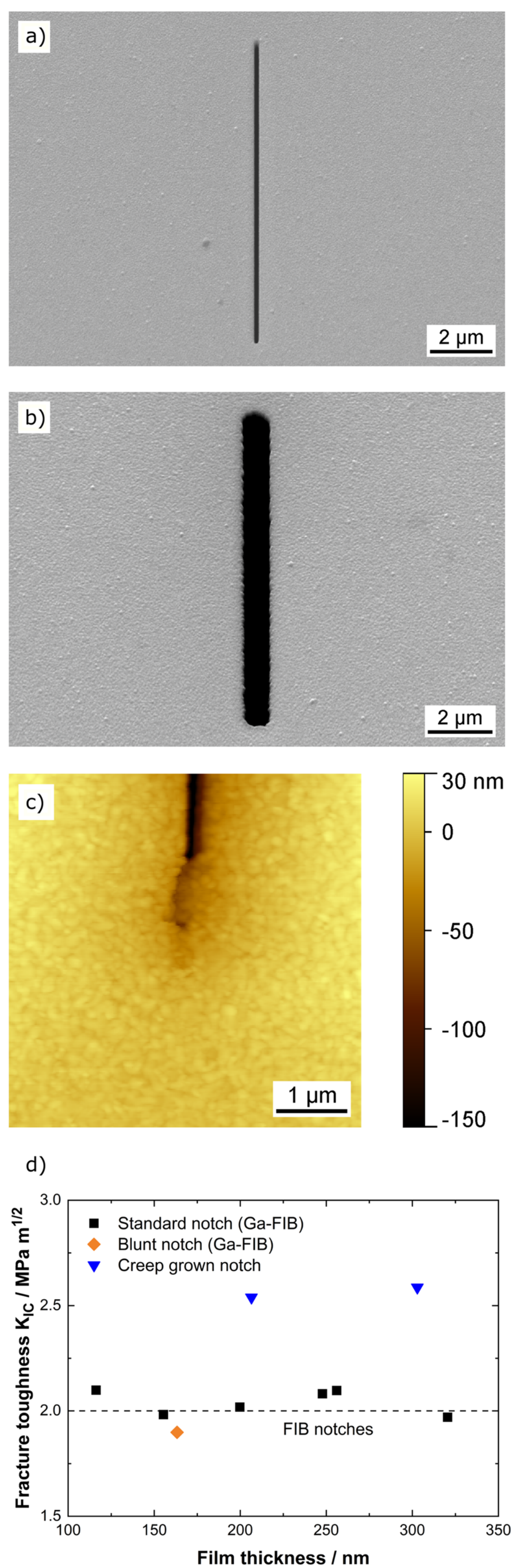

Figure 3: Effect of notch geometry resulting from Ga-FIB preparation. Secondary electron micrographs of (a) A standard notch (radius: 50–90 nm) in a 150-nm-thick gold film. (b) An intentionally blunt notch with tip radius of 450 nm. (c) AFM micrograph of a pre-crack grown by creep loading a FIB-notched membrane. The creep-grown crack extends past the FIB-affected area around the slit. (d) Fracture toughness measurements for the different notch geometries. The offset compared to Fig. 1 stems from microstructural differences between both production batches. The K_{IC} thickness independence is likely a consequence of the interplay between the geometrical thickness effect [26, 43, 44] and the yield strength dependence [28]—itself size dependent—on the fracture toughness.

the material and the implanted dose of ions [61], which further scales with the beam current and exposure time. There are many examples of a gallium-induced embrittled zone in the literature. Best et al. used Ga^+, Xe^+, and He^+ beams to prepare notches for fracture toughness measurements on micro-cantilevers of CrN [61]. They observed a smaller fracture toughness when the cantilevers were notched by Xe-FIB instead of Ga-FIB. The physical origin of this effect was not totally accounted for in their study. Furthermore, Xiao et al. demonstrated that the mechanical properties of aluminum micropillars prepared by Xe-FIB and Ga-FIB clearly differed [35]. This was rationalized by the expected embrittlement of aluminum by liquid gallium. Lauener et al. [62] observed the opposite effect from Best et al. [61], where the fracture toughness of Si micropillars fractured by indentation pillar splitting was higher for pillars milled with Xe^+ compared to Ga^+ ions. This disparity increased with decreasing pillar size, and this was rationalized by the increase in residual stress from the larger beam tails of the Xe-FIB as the pillar diameter decreased. In terms of dose, although the 250-nm-thick gold films might be expected to be the most affected by gallium-induced embrittlement due to their long processing time, the fracture toughness measurements by Xe-FIB and Ga-FIB were virtually identical (see Fig. 1c). Therefore, the low fracture toughness of the gold films [26–28] cannot be ascribed to gallium embrittlement. Granted, while xenon ions are heavier and have a lower penetration depth than gallium ions of the same energy (see Fig. 5), they also lead to greater amorphization of the surface layer [63]. However, since xenon is a noble gas, it is not expected to bond or react with gold atoms and weaken the film. Instead, xenon rather tends to form nanometer-large bubbles, as was observed in silicon [64]. Similar bubbles are expected to be formed during Ne-FIB processing. The primary difference between Ne ions and Ga-FIB or Xe-FIB is that neon ions are lighter and thus penetrate deeper into the target material (see Fig. 5).

Another significant factor which influences the extent of FIB damage is the milling strategy employed during sample

© The Author(s) 2021

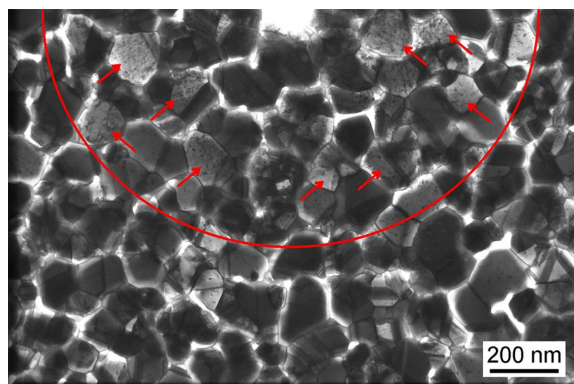

Figure 4: Scanning transmission electron micrograph of the tip of a FIB-milled notch in a 56-nm-thick freestanding gold thin film. The red arrows highlight grains in which FIB damage is visible.

preparation. Different milling strategies can result in significant variation in the dose of implanted ions received by the sample, as demonstrated by Hütsch & Lilleodden for annular and lathe milling on Mg [65]. The implantation is a function of the duration of the beam in the vicinity of the sample surface, the angle of incidence, beam current, focus of the beam (beam tails) et cetera. This is particularly relevant for the present work, as the films are milled through their total thickness using a simple line cut at normal incidence. This means that no material remains which had experienced normal implantation from the beam, unlike top-down milled notches in other testing geometries, such as micro-cantilevers [57, 66, 67]. Here, the damage inflicted to the material around the notch mostly originates from the tails of the ion beams. The sharper notch produced by the Ne-FIB—visible in Fig. 1—is the consequence of the tails of a Ne^+ beam being generally smaller than those of a typical Ga^+ or Xe^+ beam. This is because of the narrower current distribution that can be ascribed to its smaller source and spot size [68]. Thus, it is likely that the lateral dimension of the damage-affected zone is smaller with Ne-FIB than with Ga-FIB and Xe-FIB. Apart from this, the inflicted damage is very similar, namely amorphization of the surface layer and an increase of point defect density that might result in clusters or dislocation structures [53]. Nonetheless, the Ga-FIB, Xe-FIB—and to a lesser extent Ne-FIB—based measurements are in very good agreement. This is remarkable, not only because it rules out gallium-induced embrittlement, but also because the geometry of the notches strongly differs, with Xe-FIB yielding the coarsest notches and Ne-FIB the sharpest one, see Fig. 1a–c.

The independence of the fracture toughness measurement from the notch geometry can be rationalized by the intergranular character of crack propagation, previously evidenced in [26, 27]. It is likely that cracks initiate from a favorably oriented grain boundary ahead of the notch. As long as at least one such grain boundary is present at the notch, the fracture toughness measurement should not be affected by the actual notch tip radius. Under this assumption, the slightly lower fracture toughness of the specimen with a blunt notch (see Fig. 3d) can be explained

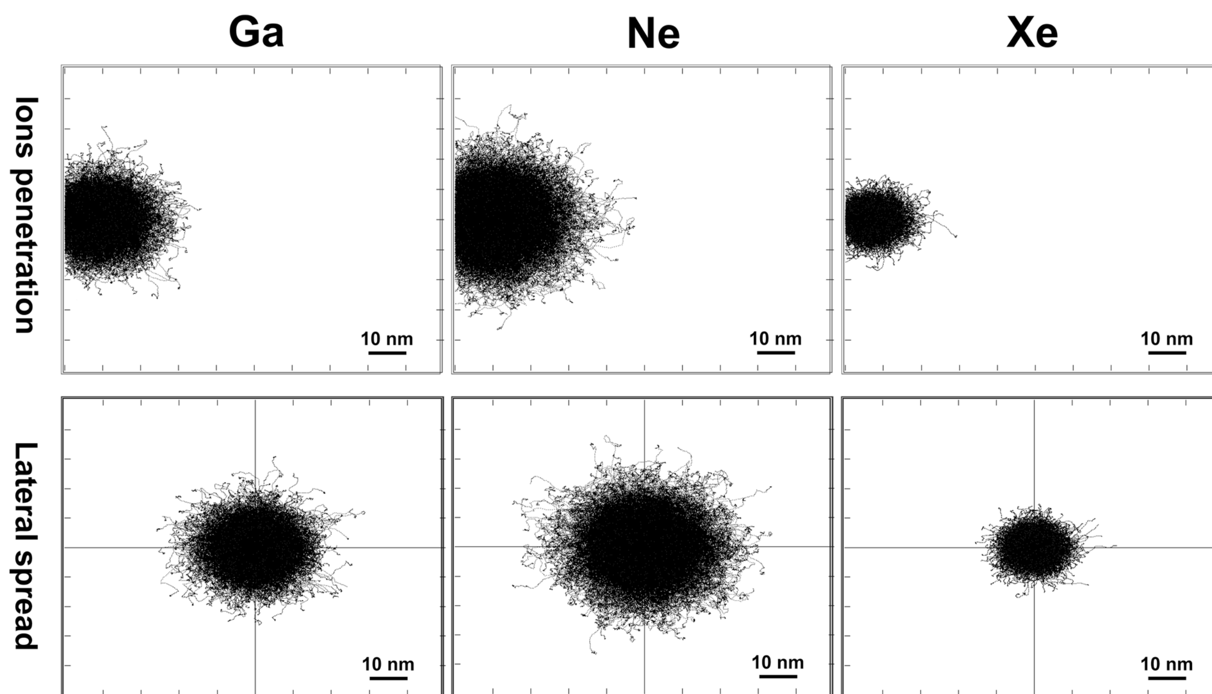

Figure 5: Monte Carlo simulations showing the extent of ion damage during irradiation of a 100-nm gold film with (a) gallium ions at 30 keV, (b) neon ions at 25 keV, (c) Xenon ions at 30 keV. 10,000 counts were simulated with SRIM [51].

© The Author(s) 2021

by the presence of more grain boundaries in front of a notch, which increases the likelihood that one of them is favorably oriented for crack initiation. Note that the sensitivity of crack nucleation and propagation on the microstructure present in front of the notch certainly accounts for much of the scatter in the data. Within this scatter, the fracture toughness measurement does not appear to be sensitive to the notch geometry or to damage specific to an ion species. A small effect cannot be ruled out, but it is concealed by larger sources of influence, such as the yield stress and hardening behavior of the film, which control the necking process in front of the notch [28].

Conclusions

The fracture toughness of gold thin films measured by bulge testing was found to be insensitive to the ion species of the focused ion beam (FIB) used for milling the pre-notch. One reason for this is that none of the main ion species (Ga^+, Ne^+, Xe^+) is likely to cause grain boundary embrittlement by chemically binding to gold, such as in gallium–aluminum. Furthermore, the through-thickness geometry of the slit ensures that there is no remaining contamination from normal exposure to the beam itself. The amount of FIB damage is reduced to that originating from the beam tails. Still, the different FIB technologies introduce different amounts of point defects in front of the notch, which are furthermore spread over different distances. They also yield very different notch radii. The K_{IC} measurements are likely unaffected by this, because a crack typically nucleates at a favorably oriented grain boundary present at the notch. It appears to make little difference whether the density of point defects is high or low around this grain boundary. For these reasons, bulge testing of gold thin films results in consistent fracture toughness measurements irrespective of the ion species that was used.

Materials and methods

The gold thin film specimens were produced by physical vapor deposition onto a 4 by 1 mm sacrificial SiN_x carrier membrane (Silson Ltd, UK), using a custom-built thermal evaporation unit. The films were deposited at a rate of 0.6 Å/s on a rotating substrate, and the substrate temperature was maintained at 120 °C during the process. Substrate heating was immediately switched off after completion. The microstructure of the films was columnar (see Fig. 6), with a surface roughness (R_a) of about 2.7 nm. The average in-plane grain size is close to the film thickness. The FIB-milled cross-section (shown in Fig. 6b) indicates a *zone II* structure with mostly columnar grains but also with some smaller and V-shaped grains [69, 70]. The films were finally made freestanding by selectively removing the SiN_x sacrificial by reactive ion etching (RIE) for 3 min by applying a 30 sccm flow of CF_4 at 12.67 Pa and a RF power of 100 W at 20 °C.

The next step consisted into introducing a slit in the center of the membranes by focused ion beam milling (FIB), so as to localize the fracture initiation. Unlike publications [26–28, 42], this fabrication step was not limited to using a Ga-FIB. Some of the films were also notched by Xe-FIB and Ne-FIB in order to investigate the effect of the ion species on FIB-induced damage on the resulting fracture toughness.

The reference Ga-FIB slits were fabricated with a 1540 CrossBeam workstation (Carl Zeiss Microscopy GmbH, Jena, Germany) equipped with a standard liquid metal ion source (LMIS). The notches were typically prepared with an ion current of 10 pA at an acceleration voltage of 30 kV. In order to minimize ion damage, beam alignment was performed at remote locations of the sample, where the film is supported by the silicon frame. The freestanding region of the film was only imaged by the electron beam and was never exposed to the ion beam but for milling operations. Milling regular through-thickness notches took 5 to 80 s depending on the film thickness. The resulting notches were typically 100–360 nm wide. After milling, the exact length of each notch was measured from an electron micrograph. On

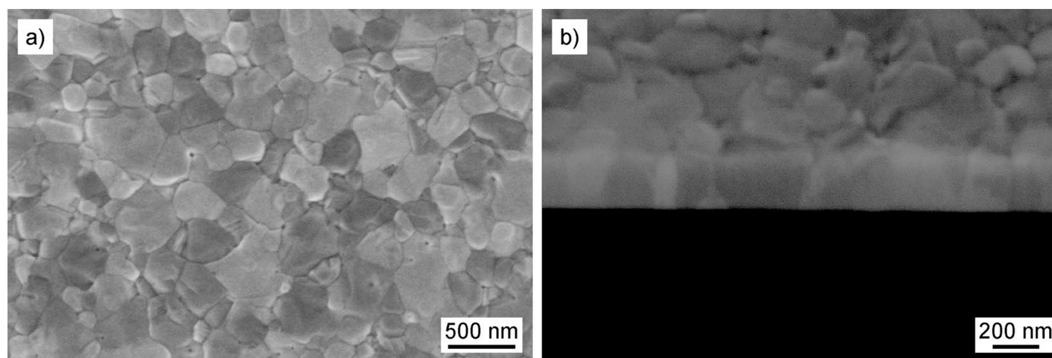

Figure 6: Secondary electron micrograph of (a) the surface of a 200-nm-thick gold film, (b) FIB cross-section of the same film. The average grain size is 220 nm. Most of the grains extend through the full thickness of the film, as typical for a zone *II* microstructure.

© The Author(s) 2021

one occasion, a pre-crack was subsequently grown from both ends of the FIB slit by creep loading the membrane at very low pressure (5–10 kPa). Its creep-driven growth was monitored in-situ in an AFM to ensure that the final crack extended beyond the FIB-affected zone present around the original notch.

An Orion NanoFab system (Carl Zeiss Microscopy GmbH, Jena, Germany) at the Max Planck Institute for the Physics of Light (Erlangen, Germany) was used to prepare notches by Ne-FIB in 100, 200, and 300-nm thick membranes. The ion beam in this system is generated by applying a high electric field to a very sharp tungsten needle with typically only three atoms (a trimer) at its apex. At the same time, the needle is surrounded by neon gas. The electric field at the tungsten trimer is sufficiently high to ionize the neon atoms in its vicinity. This gas field ionization source (GFIS) is not as stable as the LMIS used in Ga-FIB systems. Very high fields are required for the ionization of neon atoms, which raises two challenges. First, it becomes very likely that impurity atoms adhere to the tungsten tip. These may act as alternative apexes, which reduce the intensity of Ne^+ ions generated at the main tungsten trimer. Second, the tungsten trimer itself is not fully stable at such very high electric field levels. Voltage pulses, which can be applied to remove impurity atoms or excess tungsten atoms can also cause the atoms of the trimer to evaporate. However, when a firm trimer can be formed, stable operation of the source is possible over several hours. The Ne^+ ions extracted from the source are finally accelerated in an electric field and focused by an electron optics system. In comparison to Ga^+ ions, they can be focused to smaller spot sizes with smaller beam tails [54] and are typically used to mill finer features. For milling the notches, a neon gas pressure of 6.66×10^{-6} mbar was maintained at the ion source. Ion currents between 5 and 7 pA were used at an acceleration voltage of 25 kV. A 10-µm long and 1-nm wide line was scanned by the Ne^+ beam with a step size of 0.25 nm and a dwell time of 1 µs. The milling progress was estimated by monitoring the intensity of the generated secondary electrons. A sudden decrease in this intensity followed by a plateau indicated that milling was completed with the notch extending through the whole thickness of the film. Milling took about 30 to 250 s, respectively, for 100 and 300-nm-thick Au membranes. The resulting notches were 50–110 nm wide. Apart from milling operations, the gold membrane was never exposed to the Ne^+ ion beam. Imaging for alignment and centering purposes was done with a 3 pA He^+ beam at 25 kV, since there is no electron beam available in the system. As a matter of precaution, because He^+ ions can lead to swelling of the exposed material, the beam alignment was performed on the silicon substrate frame outside the membrane area.

The Xe-FIB notches were prepared with a Fera system (Tescan, Brno, Czech Republic) in the microscopy center, ScopeM, at ETH Zurich, Switzerland. In this instrument, the xenon plasma is generated by electron cyclotron resonance (ECR), which couples a magnetic field with microwaves. This technology results not only in faster milling rates, but also a larger spot size than conventional Ga-FIBs. Notching was performed with an ion current of 100 pA at an acceleration voltage of 30 kV. Milling a 10-µm-long notch through a 250-nm-thick polycrystalline gold film took 3 to 4 s.

Mechanical testing of the notched specimens was performed with a custom-built bulge tester previously described in [26–28]. The membranes were pressurized at a rate of 250 Pa/s until failure occurred. The stress at failure was calculated from the raw pressure–displacement data using the model by Vlassak et al. [71], taking into account the machine compliance. The fracture toughness was subsequently evaluated using Irwin's model [72], as advocated by [40–42]. More details about the experimental parameters can be found in [26–28].

Microstructural characterization of the samples was performed with a 1540 CrossBeam workstation (Carl Zeiss Microscopy GmbH, Jena, Germany). Scanning transmission electron microscopy (STEM) imagining was performed with a Helios NanoLab 600i dual beam workstation (FEI, Hillsboro OR, USA).

The Monte Carlo simulations were performed with the SRIM (Stopping and Range of Ions in Matter) software package [51]. A 100-nm-thick gold target was exposed to ion irradiation by 10,000 gallium ions at 30 keV, neon ions at 25 keV or Xenon ions at 30 keV. The trajectory of the ions was plotted as a function of depth, as well as laterally.

Acknowledgments

We acknowledge technical support by Dr. Anke Dutschke (Zeiss GmbH) for sample preparation with the Ne-FIB and Dr. Joakim Reuteler (ScopeM, ETH Zurich) for sample preparation with the Xe-FIB.

Funding

The authors acknowledge financial support from the Deutsche Forschungsgemeinschaft (DFG) through the research training group GRK1896 “In-situ Microscopy with Electrons, X-rays and Scanning Probes” and through the Cluster of Excellence “Engineering of Advanced Materials” (EXC315, including Bridge Funding). This research used resources from the “Center for Nanoanalysis and Electron Microscopy” (CENEM) at FAU Erlangen. Open Access funding enabled and organized by Projekt DEAL.

Open access

This article is licensed under a Creative Commons Attribution 4.0 International License, which permits use, sharing, adaptation, distribution and reproduction in any medium or format, as long as you give appropriate credit to the original author(s)

© The Author(s) 2021

and the source, provide a link to the Creative Commons licence, and indicate if changes were made. The images or other third party material in this article are included in the article's Creative Commons licence, unless indicated otherwise in a credit line to the material. If material is not included in the article's Creative Commons licence and your intended use is not permitted by statutory regulation or exceeds the permitted use, you will need to obtain permission directly from the copyright holder. To view a copy of this licence, visit http://creativecommons.org/licenses/by/4.0/.

References

1. D.S. Gianola, A. Sedlmayr, R. Mnig, C.A. Volkert, R.C. Major, E. Cyrankowski, S.A.S. Asif, O.L. Warren, O. Kraft, In situ nanomechanical testing in focused ion beam and scanning electron microscopes. Rev. Sci. Instrum. **82**(6), 063901 (2011)
2. G. Dehm, B.N. Jaya, R. Raghavan, C. Kirchlechner, Overview on micro- and nanomechanical testing: new insights in interface plasticity and fracture at small length scales. Acta Mater. **142**, 248 (2018)
3. D. Kiener, C. Motz, T. Schoeberl, M. Jenko, G. Dehm, Determination of mechanical properties of copper at the micron scale. Adv. Eng. Mater. **8**(11), 1119 (2006)
4. D. Kiener, C. Motz, W. Grosinger, D. Weygand, R. Pippan, Cyclic response of copper single crystal micro-beams. Scr. Mater. **63**(5), 500 (2010)
5. P.J. Imrich, C. Kirchlechner, D. Kiener, G. Dehm, Internal and external stresses: In situ TEM compression of Cu bicrystals containing a twin boundary. Scr. Mater. **100**, 94 (2015)
6. S.H. Oh, M. Legros, D. Kiener, G. Dehm, In situ observation of dislocation nucleation and escape in a submicrometre aluminium single crystal. Nat. Mater. **8**(2), 95 (2009)
7. F. Mompiou, M. Legros, A. Sedlmayr, D.S. Gianola, D. Caillard, O. Kraft, Source-based strengthening of sub-micrometer Al fibers. Acta Mater. **60**(3), 977 (2012)
8. D.S. Gianola, S. Van Petegem, M. Legros, S. Brandstetter, H. Van Swygenhoven, K.J. Hemker, Stress-assisted discontinuous grain growth and its effect on the deformation behavior of nanocrystalline aluminum thin films. Acta Mater. **54**(8), 2253 (2006)
9. G. Dehm, C. Motz, C. Scheu, H. Clemens, P.H. Mayrhofer, C. Mitterer, Mechanical size-effects in miniaturized and bulk materials. Adv. Eng. Mater. **8**(11), 1033 (2006)
10. D. Kiener, W. Grosinger, G. Dehm, R. Pippan, A further step towards an understanding of size-dependent crystal plasticity: in situ tension experiments of miniaturized single-crystal copper samples. Acta Mater. **56**(3), 580 (2008)
11. C. Kirchlechner, D. Kiener, C. Motz, S. Labat, N. Vaxelaire, O. Perroud, J.-S. Micha, O. Ulrich, O. Thomas, G. Dehm, J. Keckes, Dislocation storage in single slip-oriented Cu micro-tensile samples: new insights via X-ray microdiffraction. Philos. Mag. **91**(7–9), 1256 (2011)
12. J.P. Liebig, M. Göken, G. Richter, M. Mackovic, T. Przybilla, E. Spiecker, O.N. Pierron, B. Merle, A flexible method for the preparation of thin film samples for in situ TEM characterization combining shadow-FIB milling and electron-beam-assisted etching. Ultramicroscopy **171**, 82 (2016)
13. B. Merle, H.W. Höppel, Microscale high-cycle fatigue testing by dynamic micropillar compression using continuous stiffness measurement. Exp. Mech. **58**(3), 465 (2018)
14. S. Gabel, B. Merle, Small-scale high-cycle fatigue testing by dynamic microcantilever bending. MRS Commun. **10**(2), 332 (2020)
15. J.R. Greer, W.D. Nix, Nanoscale gold pillars strengthened through dislocation starvation. Phys. Rev. B Condens. Matter Mater. Phys. **73**(24), 245410 (2006)
16. S.C. Pun, W. Wang, A. Khalajhedayati, J.D. Schuler, J.R. Trelewicz, T.J. Rupert, Nanocrystalline Al-Mg with extreme strength due to grain boundary doping. Mater. Sci. Eng. A **696**, 400 (2017)
17. S. Korte, W.J. Clegg, Micropillar compression of ceramics at elevated temperatures. Scr. Mater. **60**(9), 807 (2009)
18. J. Schwiedrzik, R. Raghavan, A. Bürki, V. Lenader, U. Wolfram, J. Michler, P. Zysset, In situ micropillar compression reveals superior strength and ductility but an absence of damage in lamellar bone. Nat. Mater. **13**(7), 740 (2014)
19. Y. Xiao, Y. Zou, A.S. Sologubenko, R. Spolenak, J.M. Wheeler, Size-dependent strengthening in multi-principal element, face-centered cubic alloys. Mater. Des. **193**, 108786 (2020)
20. D. Kiener, P. Hosemann, S.A. Maloy, A.M. Minor, In situ nanocompression testing of irradiated copper. Nat. Mater. **10**(8), 608 (2011)
21. N.V. Malyar, H. Springer, J. Wichert, G. Dehm, C. Kirchlechner, Synthesis and mechanical testing of grain boundaries at the micro and sub-micro scale. Mater. Test. **61**(1), 5 (2019)
22. J.P. Liebig, S. Krauß, M. Göken, B. Merle, Influence of stacking fault energy and dislocation character on slip transfer at coherent twin boundaries studied by micropillar compression. Acta Mater. **154**, 261 (2018)
23. S. Krauß, T. Schieß, M. Göken, B. Merle, Revealing the local fatigue behavior of bimodal copper laminates by micropillar fatigue tests. Mater. Sci. Eng. A **788**, 139502 (2020)
24. N.V. Malyar, J.S. Micha, G. Dehm, C. Kirchlechner, Dislocation-twin boundary interaction in small scale Cu bi-crystals loaded in different crystallographic directions. Acta Mater. **129**, 91 (2017)
25. P.J. Imrich, C. Kirchlechner, C. Motz, G. Dehm, Differences in deformation behavior of bicrystalline Cu micropillars containing a twin boundary or a large-angle grain boundary. Acta Mater. **73**, 240 (2014)

© The Author(s) 2021

26. E.I. Preiß, B. Merle, M. Göken, Understanding the extremely low fracture toughness of freestanding gold thin films by in-situ bulge testing in an AFM. Mater. Sci. Eng. A **691**, 218 (2017)
27. E.I. Preiß, H. Lyu, J.P. Liebig, G. Richter, F. Gannott, P.A. Gruber, M. Göken, E. Bitzek, B. Merle, Microstructural dependence of the fracture toughness of metallic thin films: a bulge test and atomistic simulation study on single-crystalline and polycrystalline silver films. J. Mater. Res. **34**(20), 3483 (2019)
28. E.I. Preiß, F. Gannott, M. Göken, B. Merle, Scaling of the fracture toughness of freestanding metallic thin films with the yield strength. Mater. Res. Lett. **6**(10), 607 (2018)
29. T. Kondo, K. Hiramine, H. Hirakata, K. Minoshima, Fracture toughness of freestanding copper films with a thickness of 39 nm. Eng. Fr. **200**, 521 (2018)
30. H. Hirakata, Y. Takeda, T. Kondo, K. Minoshima, Direct observation of the thickness effect on critical crack tip opening displacement in freestanding copper submicron-films by in situ electron microscopy fracture toughness testing. Int. J. Fract. **192**(2), 203 (2015)
31. I. Issa, A. Hohenwarter, R. Fritz, D. Kiener, Fracture properties of ultrafine grain chromium correlated to single dislocation processes at room temperature. J. Mater. Res. **34**(13), 2370 (2019)
32. D. Kiener, C. Motz, M. Rester, M. Jenko, G. Dehm, FIB damage of Cu and possible consequences for miniaturized mechanical tests. Mater. Sci. Eng. A **459**(1), 262 (2007)
33. S. Shim, H. Bei, M.K. Miller, G.M. Pharr, E.P. George, Effects of focused ion beam milling on the compressive behavior of directionally solidified micropillars and the nanoindentation response of an electropolished surface. Acta Mater. **57**(2), 503 (2009)
34. H. Bei, S. Shim, M.K. Miller, G.M. Pharr, E.P. George, Effects of focused ion beam milling on the nanomechanical behavior of a molybdenum-alloy single crystal. Appl. Phys. Lett. **91**(11), 111915 (2007)
35. Y. Xiao, J. Wehrs, H. Ma, T. Al-Samman, S. Korte-Kerzel, M. Göken, J. Michler, R. Spolenak, J.M. Wheeler, Investigation of the deformation behavior of aluminum micropillars produced by focused ion beam machining using Ga and Xe ions. Scr. Mater. **127**, 191 (2017)
36. Y. Xiao, V. Maier-Kiener, J. Michler, R. Spolenak, J.M. Wheeler, Deformation behavior of aluminum pillars produced by Xe and Ga focused ion beams: Insights from strain rate jump tests. Mater. Des. **181**, 107914 (2019)
37. T. Vermeij, E. Plancher, C.C. Tasan, Preventing damage and redeposition during focused ion beam milling: the “umbrella” method. Ultramicroscopy **186**, 35 (2018)
38. D. Kiener, Z. Zhang, S. Šturm, S. Cazottes, P.J. Imrich, C. Kirchlechner, G. Dehm, Advanced nanomechanics in the TEM: effects of thermal annealing on FIB prepared Cu samples. Philos. Mag. **92**(25–27), 3269 (2012)
39. S. Lee, J. Jeong, Y. Kim, S.M. Han, D. Kiener, S.H. Oh, FIB-induced dislocations in Al submicron pillars: annihilation by thermal annealing and effects on deformation behavior. Acta Mater. **110**, 283 (2016)
40. J.A. Liddle, H.A. Huggins, P. Mulgrew, L.R. Harriott, H.H. Wade, K. Bolan, Fracture strength of thin ceramic membranes. Mater. Res. Soc. Symp. Proc. **338**, 501 (1994)
41. Y. Xiang, J. McKinnell, W.-M. Ang, J.J. Vlassak, Measuring the fracture toughness of ultra-thin films with application to AlTa coatings. Int. J. Fract. **144**(3), 173 (2007)
42. B. Merle, M. Göken, Fracture toughness of silicon nitride thin films of different thicknesses as measured by bulge tests. Acta Mater. **59**(4), 1772 (2011)
43. J.I. Bluhm, A model for the effect of thickness on fracture toughness. ASTM Proc. **61**, 1324 (1961)
44. J.F. Knott, *Fundamentals of Fracture Mechanics* (Butterworth and Co., London, 1973).
45. H. Hirakata, T. Yoshida, T. Kondo, K. Minoshima, Effects of film thickness on critical crack tip opening displacement in single-crystalline and polycrystalline submicron Cu films. Eng. Fract. Mech. **159**, 98 (2016)
46. S. Jaddi, M. Coulombier, J.-P. Raskin, T. Pardoen, Crack on a chip test method for thin freestanding films. J. Mech. Phys. Solids **123**, 267 (2019)
47. H.D. Espinosa, B. Peng, A new methodology to investigate fracture toughness of freestanding MEMS and advanced materials in thin film form. J. Microelectromech. Syst. **14**(1), 153 (2005)
48. E. Hosseinian, S. Gupta, O.N. Pierron, M. Legros, Size effects on intergranular crack growth mechanisms in ultrathin nanocrystalline gold free-standing films. Acta Mater. **143**, 77 (2018)
49. D. Picard, D. Leguillon, C. Putot, A method to estimate the influence of the notch-root radius on the fracture toughness measurement of ceramics. J. Eur. Ceram. Soc. **26**(8), 1421 (2006)
50. M.D. Drory, R.H. Dauskardt, A. Kant, R.O. Ritchie, Fracture of synthetic diamond. J. Appl. Phys. **78**(5), 3083 (1995)
51. J.F. Ziegler, M.D. Ziegler, J.P. Biersack, SRIM—the stopping and range of ions in matter (2010). Nucl. Instrum. Methods Phys. Res. Sect. B Beam Interact. Mater. At. **268**(11), 1818 (2010)
52. J. Guénolé, A. Prakash, E. Bitzek, Atomistic simulations of focused ion beam machining of strained silicon. Appl. Surf. Sci. **416**, 86 (2017)
53. T.C. Pekin, F.I. Allen, A.M. Minor, Evaluation of neon focused ion beam milling for TEM sample preparation. J. Microsc. **264**(1), 59 (2016)
54. S. Tan, R. Livengood, P. Hack, R. Hallstein, D. Shima, J. Notte, S. McVey, Nanomachining with a focused neon beam: A preliminary investigation for semiconductor circuit editing and failure

© The Author(s) 2021

analysis. J. Vac. Sci. Technol. B Nanotechnol. Microelectron. Mater. Process. Meas. Phenom. **29**(6), 0604 (2011)

55. W.J. MoberlyChan, D.P. Adams, M.J. Aziz, G. Hobler, T. Schenkel, Fundamentals of focused ion beam nanostructural processing: below, at, and above the surface. MRS Bull. **32**(5), 424 (2007)
56. D.J. Barber, Radiation damage in ion-milled specimens: characteristics, effects and methods of damage limitation. Ultramicroscopy **52**(1), 101 (1993)
57. J. Ast, M. Ghidelli, K. Durst, M. Göken, M. Sebastiani, A.M. Korsunsky, A review of experimental approaches to fracture toughness evaluation at the micro-scale. Mater. Des. **173**, 107762 (2019)
58. S. Schmidt, W. Sigle, W. Gust, M. Rühle, Gallium segregation at grain boundaries in aluminium. Z. Für Met. **93**(5), 428 (2002)
59. R.P. Elliott, F.A. Shunk, The Au-Ga (Gold-Gallium) system. Bull. Alloy Phase Diagr. **2**(3), 356 (1981)
60. A.D. Norton, S. Falco, N. Young, J. Severs, R.I. Todd, Microcantilever investigation of fracture toughness and subcritical crack growth on the scale of the microstructure in Al_2O_3. J. Eur. Ceram. Soc. **35**(16), 4521 (2015)
61. J.P. Best, J. Zechner, I. Shorubalko, J.V. Oboňa, J. Wehrs, M. Morstein, J. Michler, A comparison of three different notching ions for small-scale fracture toughness measurement. Scr. Mater. **112**, 71 (2016)
62. C.M. Lauener, L. Petho, M. Chen, Y. Xiao, J. Michler, J.M. Wheeler, Fracture of Silicon: Influence of rate, positioning accuracy, FIB machining, and elevated temperatures on toughness measured by pillar indentation splitting. Mater. Des. **142**, 340 (2018)
63. R. Estivill, G. Audoit, J.-P. Barnes, A. Grenier, D. Blavette, Preparation and analysis of atom probe tips by xenon focused ion beam milling. Microsc. Microanal. **22**(3), 576 (2016)
64. K. Wittmaack, H. Oppolzer, Quantitative characterization of xenon bubbles in silicon: Correlation of bubble size with the damage generated during implantation. Nucl. Instrum. Methods Phys. Res. Sect. B Beam Interact. Mater. At. **269**(3), 380 (2011)
65. J. Hütsch, E.T. Lilleodden, The influence of focused-ion beam preparation technique on microcompression investigations. Scr. Mater. **77**, 49 (2014)
66. B.N. Jaya, C. Kirchlechner, G. Dehm, Can microscale fracture tests provide reliable fracture toughness values? A case study in silicon. J. Mater. Res. **30**(5), 686 (2015)
67. J. Ast, B. Merle, K. Durst, M. Göken, Fracture toughness evaluation of NiAl single crystals by microcantilevers—a new continuous J-integral method. J. Mater. Res. **31**(23), 3786 (2016)
68. I. Utke, P. Hoffmann, J. Melngailis, Gas-assisted focused electron beam and ion beam processing and fabrication. J. Vac. Sci. Technol. B Microelectron. Nanometer Struct. Process. Meas. Phenom. **26**(4), 1197 (2008)
69. C.R.M. Grovenor, H.T.G. Hentzell, D.A. Smith, The development of grain structure during growth of metallic films. Acta Metall. **32**(5), 773 (1984)
70. J.A. Thornton, Influence of apparatus geometry and deposition conditions on the structure and topography of thick sputtered coatings. J. Vac. Sci. Technol. **11**(4), 666 (1974)
71. J.J. Vlassak, W.D. Nix, New bulge test technique for the determination of Young's modulus and Poisson's ratio of thin films. J. Mater. Res. **7**(12), 3242 (1992)
72. G.R. Irwin, Fracture, in *Handbook of Physics* (Springer, Berlin, 1958), p. 551.

© The Author(s) 2021